Predictions for p+Pb Collisions at $\sqrt{s_{NN}} = 5$ TeV: Comparison with Data

R. Vogt (with members and friends of the JET Collaboration)

Lawrence Livermore National Laboratory, Livermore, CA 94551, USA
Physics Department, University of California, Davis, CA 95616, USA

Int. J. Mod. Phys. E 22 (2013) 1330007 [arXiv:1301.3395 [hep-ph]],
Int. J. Mod. Phys. E in press [arXiv:1605.09479 [hep-ph]]

Contributions to calculations in this talk from: J. Albacete *et al.* (rcBK, charged hadrons), F. Arleo *et al.* (J/ψ, Υ), G. Barnafoldi *et al.* (charged hadrons, forward/backward asymmetry), K. J. Eskola ($R_{p\mathrm{Pb}}$, dijets), E. G. Ferreiro (J/ψ, ψ'), H. Fujii *et al.* (J/ψ, Υ), Z.-B. Kang and J.-W. Qiu (gauge bosons), J.-P. Lansberg *et al.* (J/ψ, Υ), Z. Lin (AMPT), A. Rezaeian (b-CGC charged hadrons), V. Topor Pop *et al.* (HIJINGB$\overline{\mathrm{B}}$), I. Vitev *et al.* (jets), RV (J/ψ, Υ), X.-N. Wang *et al* (charged hadrons), B.-W. Zhang *et al* (gauge bosons),

U.S. DEPARTMENT OF ENERGY | Office of Science

Outline

- **Charged particles**
  - $dN_{\mathrm{ch}}/d\eta$
  - dN_{ch}/dp_T
  - $R_{p\mathrm{Pb}}(p_T)$
- **Jets**
  - **Dijets**
  - **Single inclusive jets**
- J/ψ **and** Υ
  - $R_{p\mathrm{Pb}}(y)$
- Z **bosons**

Model Descriptions

Saturation

Saturation: rcBK (A. Rezaeian, J. Albacete *et al*)

Gluon jet production in pA described by k_T-factorization

$$\frac{d\sigma}{dy\, d^2p_T} = \frac{2\alpha_s}{C_F}\frac{1}{p_T^2}\int d^2\vec{k}_T \phi_p^G\left(x_1;\vec{k}_T\right)\phi_A^G\left(x_2;\vec{p}_T-\vec{k}_T\right)$$

Here $x_{1,2} = (p_T/\sqrt{s})e^{\pm y}$ and unintegrated gluon density, $\phi_A^G(x_i;\vec{k}_T)$, is related to color dipole forward scattering amplitude

$$\begin{aligned}\phi_A^G\left(x_i;\vec{k}_T\right) &= \frac{1}{\alpha_s}\frac{C_F}{(2\pi)^3}\int d^2\vec{b}_T\, d^2\vec{r}_T\, e^{i\vec{k}_T\cdot\vec{r}_T}\,\nabla_T^2\mathcal{N}_A\left(x_i;r_T;b_T\right)\\ \mathcal{N}_A\left(x_i;r_T;b_T\right) &= 2\mathcal{N}_F\left(x_i;r_T;b_T\right)-\mathcal{N}_F^2\left(x_i;r_T;b_T\right)\end{aligned}$$

In k_T-factorized approach, both projectile and target have to be at small x so that CGC formalism is applicable to both

rcBK Hybrid Approach

Hybrid models that treat the projectile (forward) with DGLAP collinear factorization and target with CGC methods

Hadron cross section is proportional to $f_g(x_1,\mu_F^2)N_A(x_2,p_T/z)+f_q(x_1,\mu_F^2)N_F(x_2,p_T/z)$ **modulo fragmentation functions**

$$\begin{aligned}\frac{dN^{pA\to hX}}{d\eta d^2p_T} &= \frac{K}{(2\pi)^2}\Bigg[\int_{x_F}^1\frac{dz}{z^2}\Big[x_1f_g(x_1,\mu_F^2)N_A(x_2,\frac{p_T}{z})D_{h/g}(z,\mu_{\rm Fr})\\ &+ \Sigma_q x_1 f_q(x_1,\mu_F^2)N_F(x_2,\frac{p_T}{z})D_{h/q}(z,\mu_{\rm Fr})\Big]\\ &+ \frac{\alpha_s^{\rm in}}{2\pi^2}\int_{x_F}^1\frac{dz}{z^2}\frac{z^4}{p_T^4}\int_{k_T^2<\mu_F^2}d^2k_Tk_T^2N_F(k_T,x_2)\int_{x_1}^1\frac{d\xi}{\xi}\\ &\times \Sigma_{i,j=q,\bar q,g}w_{i/j}(\xi)P_{i/j}(\xi)x_1f_j(\frac{x_1}{\xi},\mu_F)D_{h/i}(z,\mu_{\rm Fr})\Bigg]\,.\end{aligned}$$

K **factor introduced to incorporate higher order corrections**

Inelastic term is multiplied by $\alpha_s^{\rm in}$**, different from running** α_s **in rcBK equation – in hybrid formulation, strong coupling in dilute regime (proton) can differ from that in the dense system (nucleus) but appropriate scale of** $\alpha_s^{\rm in}$ **cannot be determined without a NNLO calculation**

Factorization, renormalization and fragmentation scales assumed to be equal, $\mu_F=\mu_R=\mu_{\rm Fr}$ **with** $\mu_F=2p_T$**,** p_T **and** $p_T/2$ **to form uncertainty range for given** N **and** $\alpha_s^{\rm in}$

rcBK Equation

$N_{A(F)}$ is 2-D Fourier transform of imaginary part of dipole scattering amplitude in the fundamental (F) or adjoint (A) representation $\mathcal{N}_{A(F)}$

$\mathcal{N}_{A(F)}$ calculated using JIMWLK which simplifies to BK in the large N_c limit

Running coupling corrections to LL kernel result in rcBK equation

$$\begin{aligned}\frac{\partial \mathcal{N}_{A(F)}(r,x)}{\partial \ln(x_0/x)} &= \int d^2\vec{r}_1 \; K^{\rm run}(\vec{r},\vec{r}_1,\vec{r}_2)\left[\mathcal{N}_{A(F)}(r_1,x)+\mathcal{N}_{A(F)}(r_2,x)\right.\\ &- \left.\mathcal{N}_{A(F)}(r,x)-\mathcal{N}_{A(F)}(r_1,x)\,\mathcal{N}_{A(F)}(r_2,x)\right]\end{aligned}$$

$$\mathcal{N}(r,Y=0) = 1-\exp\left[-\frac{\left(r^2\,Q_{0s}^2\right)^\gamma}{4}\,\ln\left(\frac{1}{\Lambda\,r}+e\right)\right]$$

Last equation is initial condition with γ fixed from DIS data, $\gamma=1$ is MV initial condition, $\gamma\sim 1.1$ in fits

$Q_{0p}^2\sim 0.2$ GeV^2 in MV initial condition, smaller for other values of γ

$Q_{0A}^2\sim NQ_{0p}^2$ with $3<N<7$ in Rezaeian's calculations, Albacete *et al* let nuclear scale be proportional to the number of participants at a given b to account for geometrical fluctuations in Monte Carlo simulations

Event-by-Event Calculations

HIJING2.0 (X.-N. Wang *et al*)

Based on two-component model of hadron production, soft (string excitations with effective cross section $\sigma_{\rm soft}$) and hard (perturbative QCD) components separated by cutoff momentum p_0
LO pQCD calculation with K factor to absorb higher-order corrections

$$\frac{d\sigma_{pA}^{\rm jet}}{dy_1 d^2p_T} = K \int dy_2\, d^2b\, T_A(b) \sum_{a,b,c} x_1 f_{a/p}(x_1, p_T^2) x_2 f_{a/A}(x_2, p_T^2, b) \frac{d\sigma_{ab\to cd}}{dt}$$

Effective $2 \to 2$ scattering, $x_{1,2} = p_T(e^{\pm y_1} + e^{\pm y_2})/\sqrt{s}$

Default HIJING collisions decomposed into independent and sequential NN collisions – in each NN interaction, hard collisions simulated first, followed by soft

Since hard interactions occur over shorter time scale, HIJING2.0 also uses decoherent hard scattering (DHC) where all hard collisions are simulated first, then soft, so available energy unrestricted by soft interactions
Energy-dependent k_T broadening in HIJING

$$\langle k_T^2 \rangle = [0.14 \log(\sqrt{s}/\text{GeV}) - 0.43]\,\text{GeV}^2/c^2$$

Shadowing in HIJING

Shadowing treated as scale independent
Versions before HIJING2.0 did not differentiate between quark and gluon shadowing

$$
\begin{aligned}
f_{a/A}(x,\mu_F^2,b) &= S_{a/A}(x,\mu_F^2,b) f_{a/A}(x,\mu_F^2) \\
S_{a/A}(x) &\equiv \frac{f_{a/A}(x)}{A f_{a/N}(x)} \\
&= 1 + 1.19 \log^{1/6} A \left[x^3 - 1.2x^2 + 0.21x\right] \\
&\quad - s_a (A^{1/3}-1)^n \left[1 - \frac{10.8}{\log(A+1)}\sqrt{x}\right] e^{-x^2/0.01} \\
s_a(b) &= s_a \frac{5}{3}\left(1 - \frac{b^2}{R_A^2}\right)
\end{aligned}
$$

In HIJING2.0 the $(A^{1/3}-1)$ factor is nonlinear ($n = 0.6$) but $n = 1$ in earlier versions

Previously $s_a = s_g = s_q = 0.1$

In HIJING2.0 $s_g \neq s_q$: $s_q = 0.1$ and $s_g \sim 0.22 - 0.23$ to match LHC data

The b dependence of s_a gives some impact parameter dependence to $S_{a/A}$

HIJINGB$\overline{\text{B}}$ (V. Topor Pop *et al*)

Differs from standard HIJING in treatment of fragmentation

HIJING uses string fragmentation with constant vacuum value of $\kappa_0 = 1.0$ GeV/fm for string tension

HIJINGB$\overline{\text{B}}$ allows for multiple overlapping flux tubes leading to strong longitudinal color field (SCF) effects

SCF effects modeled by varying κ and momentum cutoff with $\sqrt{s}$ and A

Fragmentation also modified, including baryon loops to explain baryon to meson anomaly and increase strange baryon production

AMPT: A Multi-Phase Transport (Z. Lin)

AMPT is a Monte Carlo transport model for heavy ion collisions, montage of other codes

- Heavy Ion Jet Interaction Generator (HIJING) for generating the initial conditions
- Zhang's Parton Cascade (ZPC) for modeling partonic scatterings
- A Relativistic Transport (ART) model for treating hadronic scatterings

AMPT – def treats the initial condition as strings and minijets and using Lund string fragmentation

AMPT – SM treats the initial condition as partons and uses a simple coalescence model to describe hadronization

Perturbative QCD Calculations, Collinear Factorization

LO/NLO pQCD, w/out Energy Loss (G. Barnafoldi *et al*)

`kTpQCD_v2.0` assumes collinear factorization up to NLO

$$
\begin{aligned}
E_h \frac{d\sigma_h^{pp}}{d^3 p_T} &= \frac{1}{s} \sum_{abc} \int_{VW/z_c}^{1-(1-V)/z_c} \frac{dv}{v(1-v)} \int_{VW/vz_c}^{1} \frac{dw}{w} \int^{1} dz_c \\
&\times \int d^2\vec{k}_{T_1} \int d^2\vec{k}_{T_2}\; f_{a/p}(x_1, \vec{k}_{T_1}, \mu_F^2)\, f_{b/p}(x_2, \vec{k}_{T_2}, \mu_F^2) \\
&\times \left[\frac{d\widetilde{\sigma}}{dv} \delta(1-w) + \frac{\alpha_s(\mu_R)}{\pi} K_{ab,c}(\hat{s}, v, w, \mu_F, \mu_R, \mu_{\rm Fr}) \right] \frac{D_c^h(z_c, \mu_{\rm Fr}^2)}{\pi z_c^2} \; .
\end{aligned}
$$

$d\widetilde{\sigma}/dv$ is LO cross section with next-order correction term $K_{ab,c}(\hat{s}, v, w, \mu_F, \mu_R, \mu_{\rm Fr})$

Proton and parton level NLO kinematic variables are (s, V, W) and ($\hat{s}$, v, w)

k_T broadening implemented similar to previous LO calculation with

$$
\langle k_T^2 \rangle_{pA} = \langle k_T^2 \rangle_{pp} + C h_{pA}(b)
$$

$$
h_{pA}(b) = \begin{cases} \nu_A(b) - 1 & \nu_A(b) < \nu_m \\ \nu_m - 1 & \text{otherwise} \end{cases}
$$

Shadowing implemented through available parameterizations: EKS98, EPS08, HKN, and `HIJING2.0` – scale dependence included

$$
f_{a/A}(x, \mu_F^2) = S_{a/A}(x, \mu_F^2) \left[\frac{Z}{A} f_{a/p}(x, \mu_F^2) + \left(1 - \frac{Z}{A} \right) f_{a/n}(x, \mu_F^2) \right]
$$

NLO Shadowing Calculation (K. J. Eskola *et al*)

Calculate π^0 production at NLO, compared to charged particle R_{AA}

Only modifications of the parton PDFs in nuclei included

Improved spatial dependence of nPDFs on both EKS98 and EPS09 using power series expansion in the nuclear thickness function

$$r_i^A(x, Q^2, \mathbf{s}) = 1 + \sum_{j=1}^{n} c_j^i(x, Q^2) \left[T_A(\mathbf{s})\right]^j$$

They use the A dependence of the global (min bias) nPDFs to fix coefficients c_j^i

Found $n = 4$ sufficient for reproducing the A systematics

Used INCNLO package with CTEQ6M and KKP, AKK and fDSS fragmentation functions, uncertainties calculated with EPS09(s) error sets and fDSS

The modification factor $R_{p\mathrm{Pb}}$ is calculated as

$$R_{p\mathrm{Pb}}^{\pi^0}(p_T, y; b_1, b_2) \equiv \frac{\left\langle \dfrac{d^2N_{p\mathrm{Pb}}^{\pi^0}}{dp_T dy} \right\rangle_{b_1,b_2}}{\dfrac{\langle N_{\mathrm{coll}}^{p\mathrm{Pb}} \rangle_{b_1,b_2}}{\sigma_{\mathrm{in}}^{NN}} \dfrac{d^2\sigma_{\mathrm{pp}}^{\pi^0}}{dp_T dy}} = \frac{\int_{b_1}^{b_2} d^2\mathbf{b} \dfrac{d^2N_{p\mathrm{Pb}}^{\pi^0}(\mathbf{b})}{dp_T dy}}{\int_{b_1}^{b_2} d^2\mathbf{b}\, T_{p\mathrm{Pb}}(\mathbf{b}) \dfrac{d^2\sigma_{\mathrm{pp}}^{\pi^0}}{dp_T dy}}$$

b_1 and b_2 are centrality-based limits with $b_1 = 0$ and $b_2 \to \infty$ in min bias collisions

Charged particle and π^0 $R_{p\mathrm{Pb}}$ may be different because of greater baryon contribution in pA collisions, at least in some parts of phase space

Charged Particle Multiplicity and p_T Distributions: Midrapidity

CGC: Improved Results on $dN_{\rm ch}/d\eta$

The slope of $dN_{\rm ch}/d\eta$ depends on the Jacobian $y \to \eta$ transformation

Previous calculations assumed the same Jacobian in pp and p+Pb collisions

(LHS) New results based on 'tuned' Jacobian shows the sensitivity of $dN_{\rm ch}/d\eta$ to mass and p_T of final-state hadrons (note also that the convention is changed, proton beam has positive y)

(RHS) Fixed minijet mass (related to pre-handronization/fragmentation stage) is assumed – can't be extracted in CGC, problem largest on the nuclear side

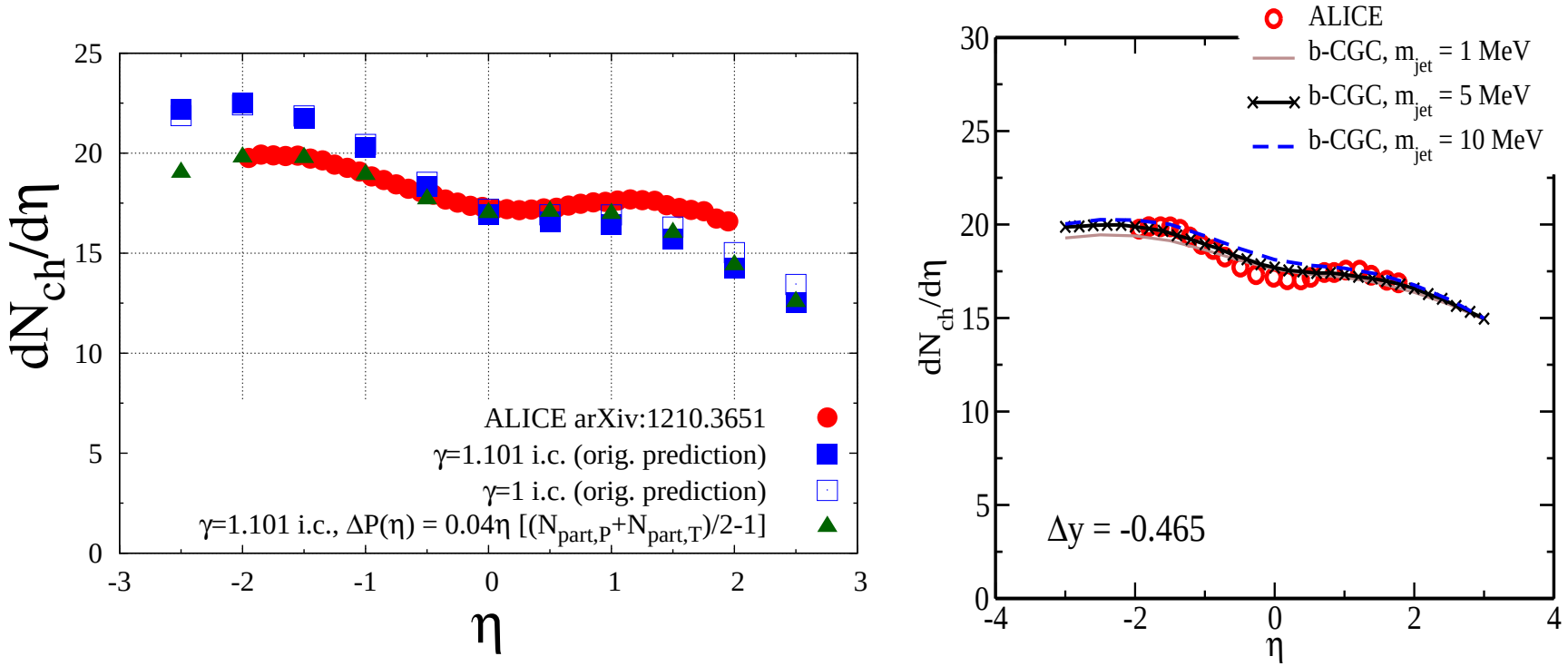

Figure 1: **Charged particle pseudorapidity distributions at $\sqrt{s_{NN}} = 5.02$ TeV with and without tuned Jacobian compared to the ALICE data (Phys. Rev. Lett. 110 (2013) 082302). Calculations by Albacete *et al.* with $\Delta P(\eta)$ are shown on the left-hand side, results changing the minijet mass in b-CGC by Rezaeian are shown on the right-hand side. Note that here the proton moves to the right (positive y).**

Centrality Dependence of $dN_{\rm ch}/d\eta$

Left-hand side compares `AMPT – def` (Z. Lin) to ATLAS data

Right-hand side shows the comparison with b-CGC: saturation scale modified to depend on impact parameter (A. Rezaeian)

Results are qualitatively similar but b-CGC more linear than data in more central collisions

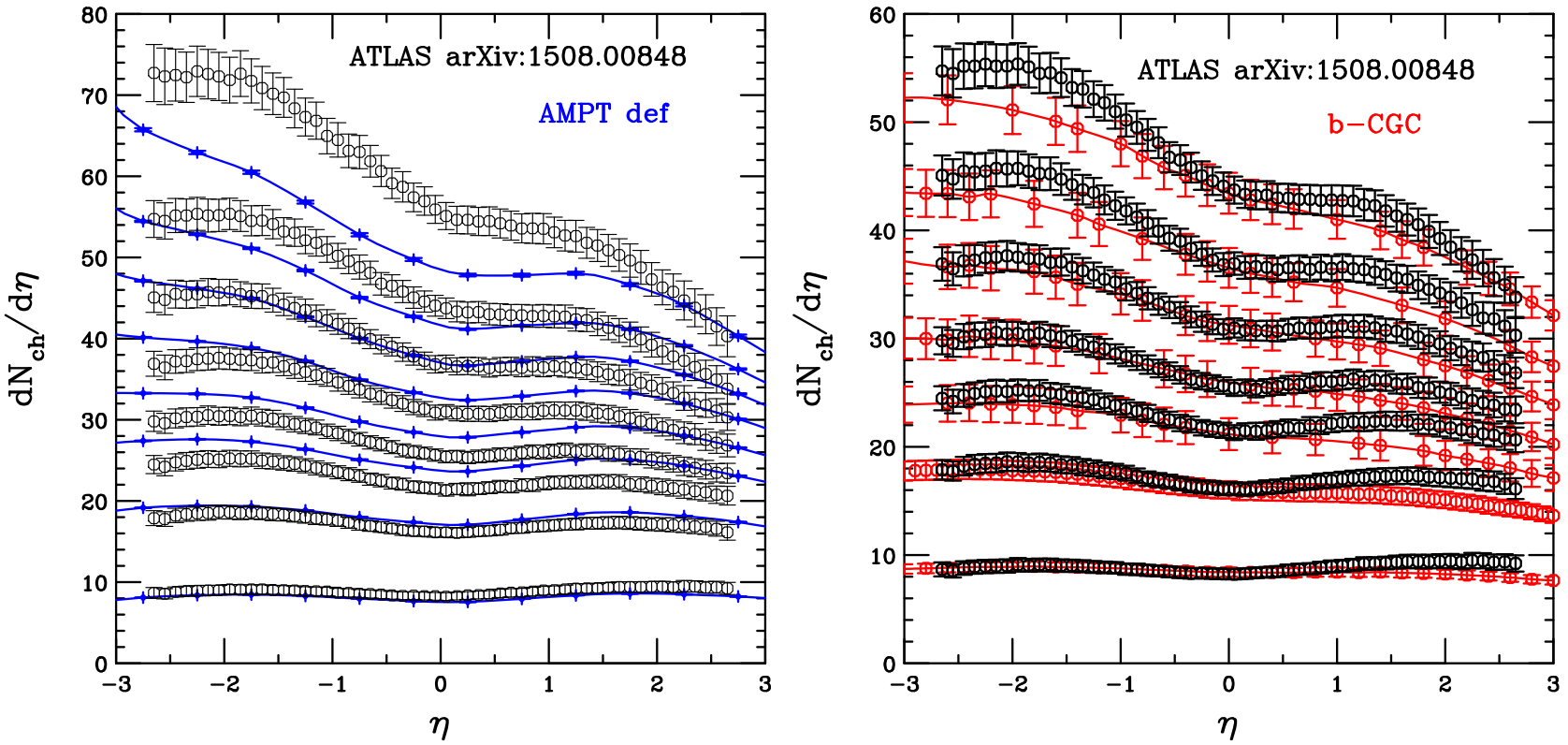

Figure 2: **The ATLAS multiplicity distributions (arXiv:1508.00848), binned in centrality, are compared to calculations with `AMPT – def` by Lin (left) and b-CGC by Rezaeian (right). There is no 0-1% b-CGC centrality calculation.**

Updates on $R_{p\mathrm{Pb}}$ at Midrapidity

The proportionality factor, N, multiplying $Q^2_{0,p}$ in the rcBK, b-CGC (Rezaeian) calculation has been narrowed down and agrees with $R_{p\mathrm{Pb}}$, better predicts $R_{p\mathrm{Pb}}$ at higher rapidity

EPS09 NLO (Eskola *et al*) agrees with ALICE and CMS data for $p_T < 20$ GeV but small (anti-)shadowing at high p_T cannot produce rise at high p_T, need measured instead of interpolated pp baseline

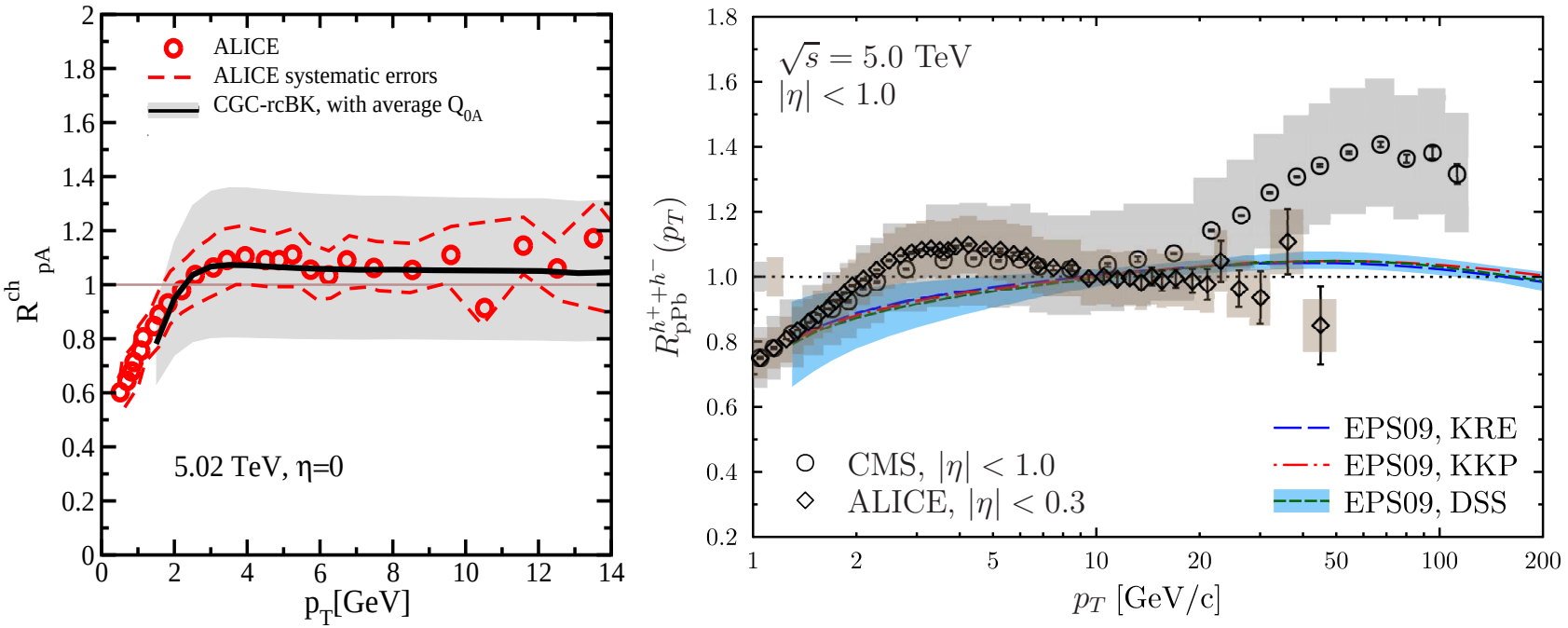

Figure 3: **Charged particle $R_{p\mathrm{Pb}}(p_T)$ calculations at $\sqrt{s_{NN}} = 5.02$ TeV at $\eta \sim 0$ are compared to the ALICE data (Phys. Rev. Lett. 110 (2013) 082302). (Left) The updated Rezaeian (rcBK) band, green curves on upper left of previous slide, adjusting range of N based on data – $R_{p\mathrm{Pb}}$ at other rapidities would be predictions. (Right) Results with EPS09 NLO modifications. The CMS data (Eur. Phys. J. C 75 (2015) 237) are shown to higher p_T.**

ALICE Charged Particle p_T Distributions

Results similar at low p_T but deviate significantly at higher p_T

AMPT agrees well with $p_T > 5$ GeV data, rcBK is better at low p_T, HIJINGB$\overline{\text{B}}$ is higher than data for $p_T > 3$ GeV

HIJING2.0 without shadowing better at low p_T, with better at high p_T

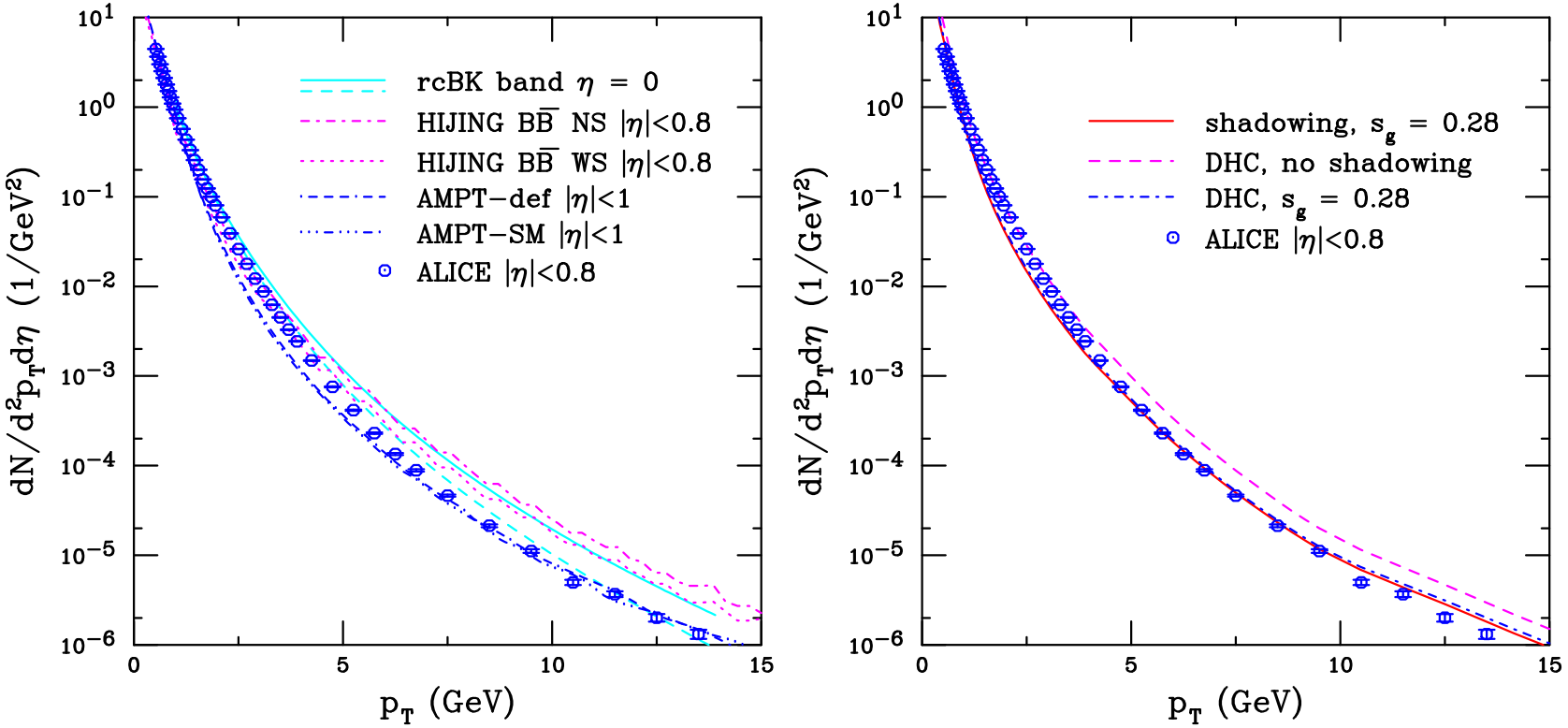

Figure 4: **(Left) Charged particle p_T distributions at $\sqrt{s_{NN}} = 5.02$ TeV. The solid and dashed cyan curves outline the rcBK band calculated by Albacete *et al.*. The magenta curves, calculated with HIJINGB$\overline{\text{B}}$2.0 are presented without (dot-dashed) and with (dotted) shadowing. The AMPT results are given by the dot-dash-dash-dashed (default) and dot-dot-dot-dashed (SM) blue curves. The data are from the ALICE Collaboration, Phys. Rev. Lett. 110 082302 (2013). (Right) The charged hadron p_T distribution in p+Pb collisions with different HIJING2.1 options is also compared to the ALICE data.**

CMS Charged Particle p_T Distributions

Agreement of calculations with CMS data similar as for ALICE data

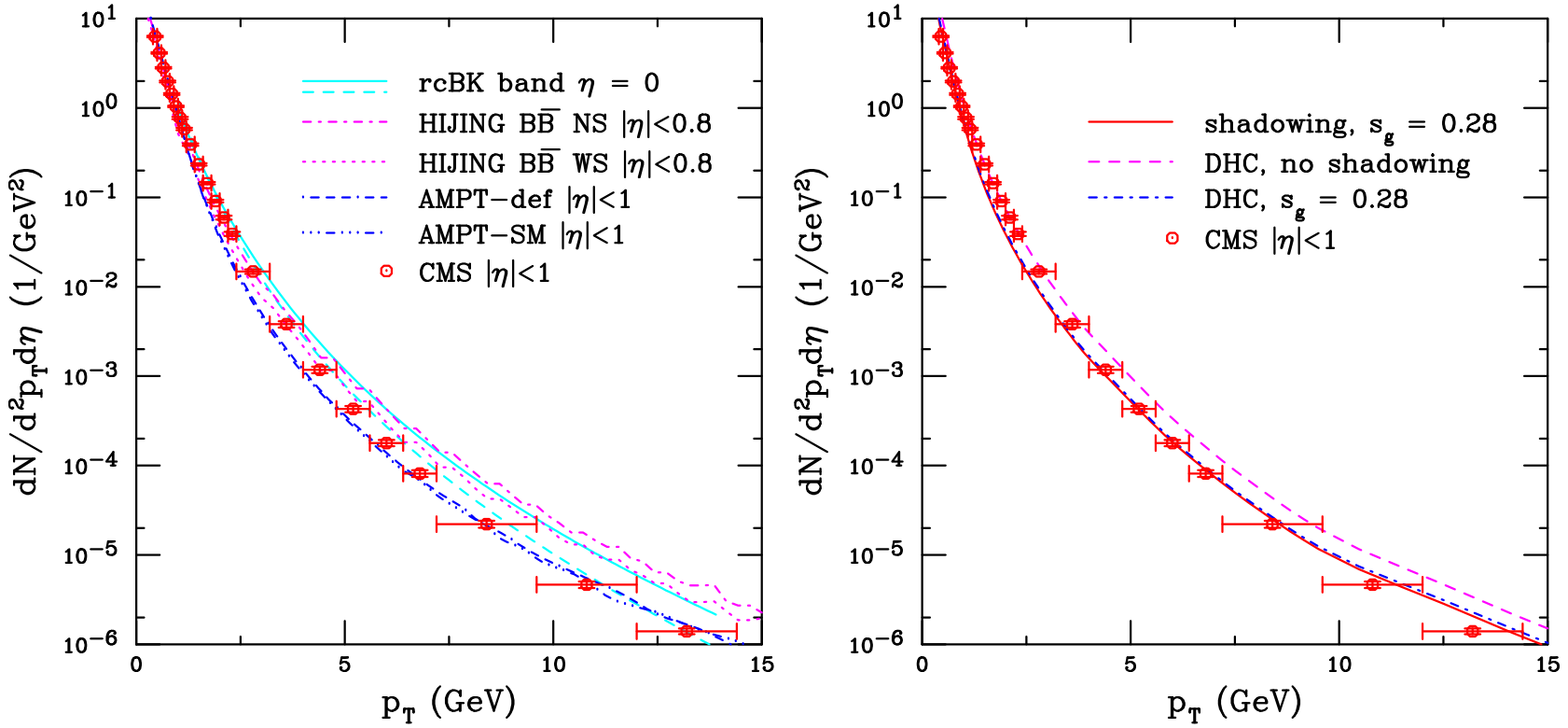

Figure 5: **(Left) Charged particle p_T distributions at $\sqrt{s_{NN}} = 5.02$ TeV. The solid and dashed cyan curves outline the rcBK band calculated by Albacete *et al.*. The magenta curves, calculated with HIJINGBB̄2.0 are presented without (dot-dashed) and with (dotted) shadowing. The AMPT results are given by the dot-dash-dash-dashed (default) and dot-dot-dot-dashed (SM) blue curves. The data are from the CMS Collaboration (Eur. Phys. J. C 75 (2015) 237). (Right) The charged hadron p_T distribution in p+Pb collisions with different HIJING2.1 options is also compared to the CMS data.**

Forward-Backward Asymmetry

$$Y_{\rm asym}(p_T) = \frac{E_h d^3\sigma^h_{p{\rm Pb}}/d^2p_T d\eta|_{\eta>0}}{E_h d^3\sigma^h_{p{\rm Pb}}/d^2p_T d\eta|_{\eta<0}} = \frac{R^h_{p{\rm Pb}}(p_T,\eta>0)}{R^h_{p{\rm Pb}}(p_T,\eta<0)}$$

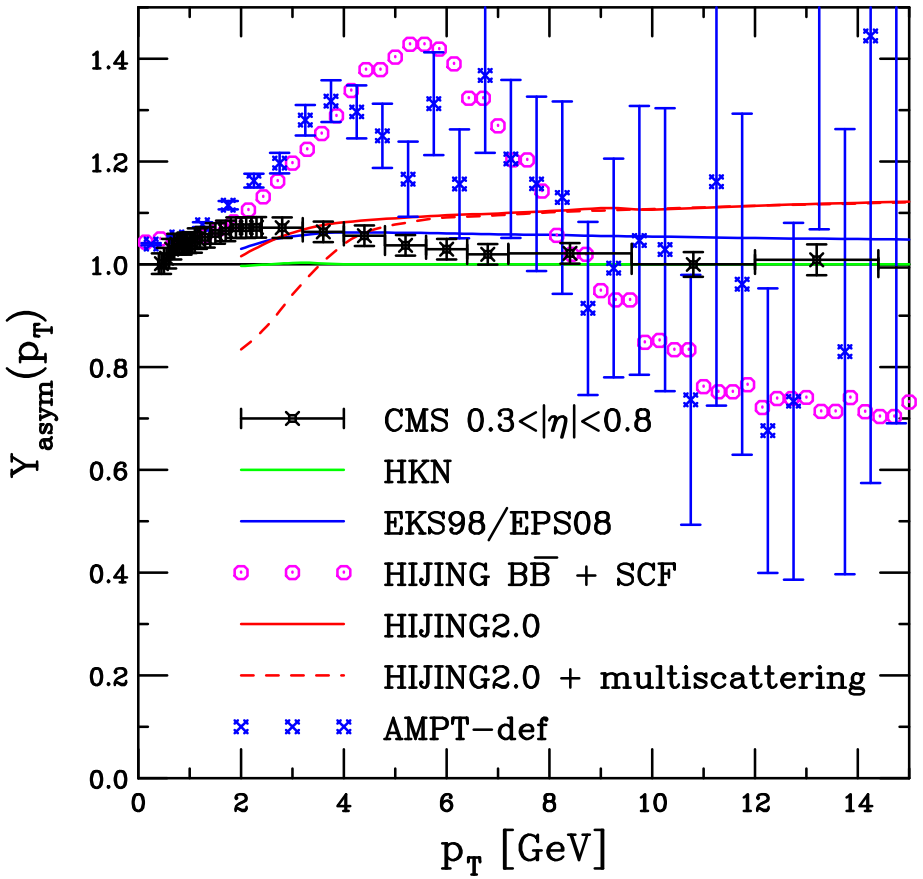

Figure 6: Predictions for the forward-backward asymmetry, $Y^h_{\rm asym}(p_T)$. Centrality independent results are shown for the HKN, EKS98 and EPS08 parameterizations (labeled MB). Minimum bias results are also shown for `HIJINGBB̄2.0` and `HIJING2.0` with multiple scattering. In addition, `HIJING2.0` results in MB collisions and for the 20% most central collisions are also shown. All these calculations were provided by Barnafoldi *et al.* The blue points are the `AMPT − def` results by Lin. The results are compared to the CMS data (Eur. Phys. J. C **75** (2015) 237) in the rapidity range $0.3 < y < 0.8$.

Jets

Dijets with EPS09 NLO

Rapidity distribution (Eskola *et al*) shows clear shift

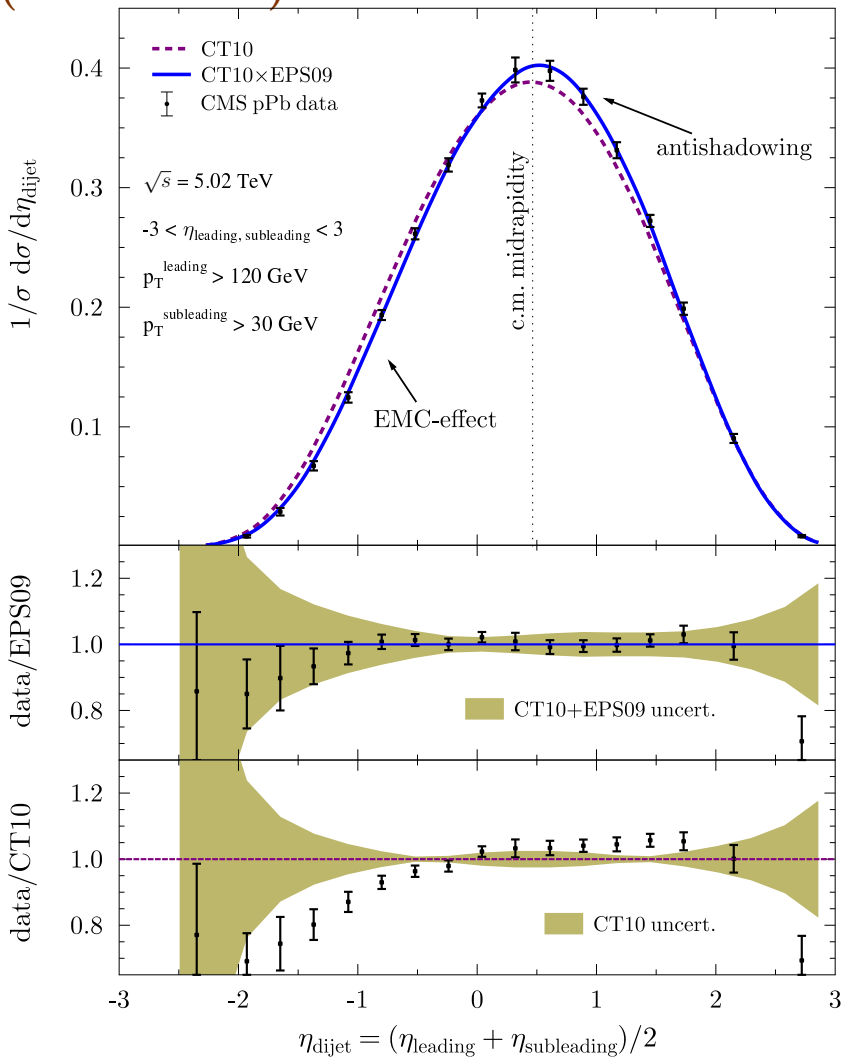

Figure 7: **The CMS dijet measurements (Eur. Phys. J. C 74 (2014) 2951) are compared to EPS09 NLO. The upper panel shows the normalized cross section as a function of η_{dijet}. The lower two panels display the ratio of the data to the CT10+EPS09 and CT10 calculations respectively, including the PDF and nPDF uncertainty bands.**

Single Inclusive Jet Production: Scaling With $p_T \cosh y$

The ATLAS data scale with $p_T \cosh y$ at forward rapidity, scaling becomes weaker at midrapidity and is broken at backward rapidity

Calculations by Kang, Vitev and Xing including cold matter energy loss exhibit the same scaling ($x_1 \propto p_T \cosh y$) but not the same curvature

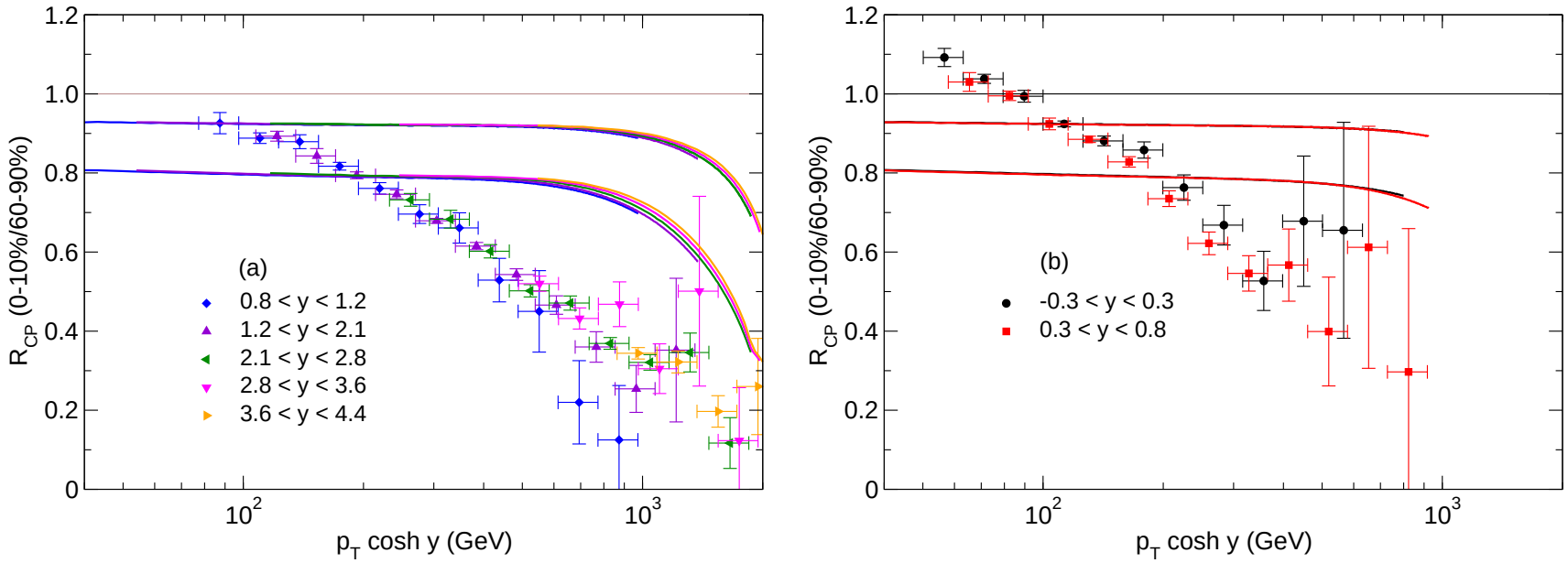

Figure 8: **Comparison of the calculated R_{CP} with the ATLAS data (Phys. Lett. B 748 (2015) 392) as a function of $p_T \cosh y$ by Kang *et al.*. In (a), the results at forward rapidities ($0.8 < y < 1.2$ (blue diamonds), $1.2 < y < 2.1$ (maroon upward-pointing triangles), $2.1 < y < 2.8$ (green left-pointing triangles), $2.8 < y < 3.6$ (magenta downward-pointing triangles), and $3.6 < y < 4.4$ (orange right-pointing triangles) are shown. In (b), results near midrapidity are shown ($-0.3 < y < 0.3$ (black circles) and $0.3 < y < 0.8$ (red squares)). The upper and lower limits of the calculation for each rapidity region overlap each other.**

J/ψ and Υ

Final-State Energy Loss (Arleo and Peigne)

Arleo and Peigne fit an energy loss parameter that also depends on L_A to E866 data and uses the same parameter for other energies

$$\frac{1}{A}\frac{d\sigma_{pA}(x_F)}{dx_F} = \int_0^{E_p-E} d\epsilon P(\epsilon)\frac{d\sigma_{pp}(x_F+\delta x_F(\epsilon))}{dx_F}$$

There is no production model, only a parameterization of the pp cross section

$$\frac{d\sigma_{pp}}{dp_T dx} = \frac{(1-x)^n}{x}\left(\frac{p_0^2}{(p_0^2+p_T^2)}\right)^m$$

Parameters n and m are fit to pp data, $n \sim 5$ at $\sqrt{s} = 38.8$ GeV, 34 at 2.76 TeV

Including shadowing as well as energy loss modifies the energy loss parameter, no significant difference in shape of fit at fixed-target energy but significant difference at higher $\sqrt{s}$

Backward x_F/y effect is large for this scenario

Initial-State Modifications (RV, Lansberg, and Fujii)

We use charm mass and scale fit to total charm data to calculate quarkonium in the color evaporation model (CEM) at NLO

The EPS09 NLO sets are employed; all sets are used and the uncertainties on the shadowing obtained by adding in quadrature

EPS09 NLO has weaker shadowing effect than the EPS09 LO at forward rapidity due to different low x behavior of PDFs

Lansberg and collaborators use LO color singlet model (CSM) to calculate production

Using LO CSM modifies R_{pA} relative to LO CEM due to shadowing because LO CEM has $p_T = 0$ for the J/ψ (y dependence only), other differences include mass and scale values used

Uncertainites in the shadowing result shown are from two particular EPS09 sets that give the minimum and maximum magnitudes of gluon shadowing, not from taking all sets in quadrature

CGC calculations by Fujii *et al.* are made only in the forward direction where x_2 (in Pb nucleus) is small

Uncertainty comes from varying the saturation scale, $Q^2_{0\mathrm{sat},A} \sim (4-6)Q^2_{0\mathrm{sat},p}$ and the quark masses, $1.2 < m_c < 1.5$ GeV and $4.5 < m_b < 4.8$ GeV

$R_{p\mathrm{Pb}}(y)$ for J/ψ and Υ

NLO shadowing does not describe curvature of data, LO band is larger due to greater uncertainty of EPS09 LO (only min/max used in Lansberg calculation)

Energy loss alone does well for J/ψ $R_{p\mathrm{Pb}}$ but stronger curvature for R_{FB}, unclear for Υ

CGC + CEM (Fujii) below data, CGC + NRQCD (not shown) may agree better

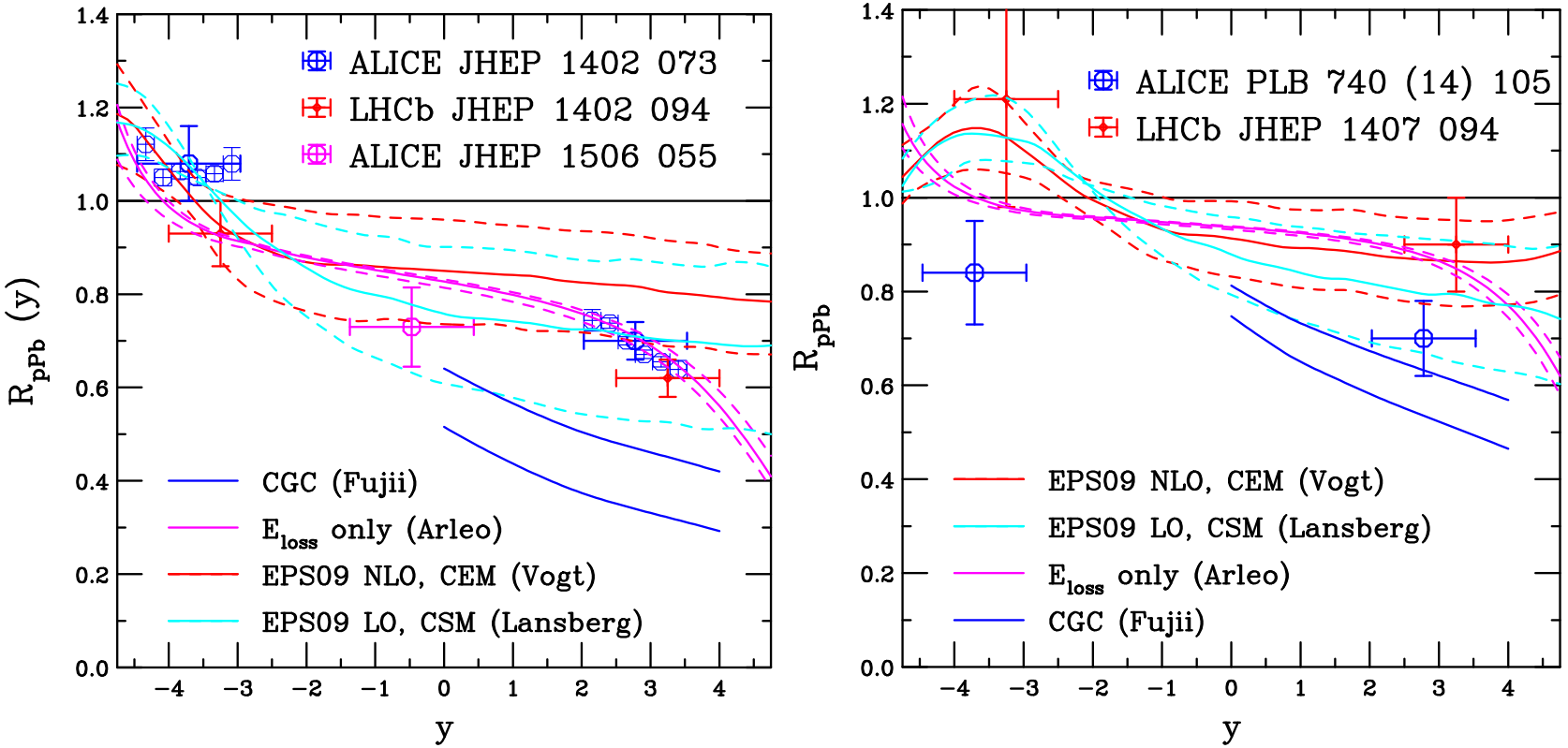

Figure 9: **(Left) The $R_{p\mathrm{Pb}}$ ratio for J/ψ as a function of y. The dashed red histogram shows the EPS09 NLO CEM uncertainties. The EPS09 LO CSM calculation by Lansberg *et al.* is shown in cyan. The energy loss calculation of Arleo and Peigne is shown in magenta. The upper and lower limits of the CGC calculation by Fujii *et al* are in blue at forward rapidity. (Right) The $R_{p\mathrm{Pb}}$ ratio for Υ as a function of y. The dashed red histogram shows the EPS09 NLO CEM uncertainties. The EPS09 LO CSM calculation by Lansberg *et al.* is shown in cyan. The energy loss calculation of Arleo and Peigne is shown in magenta. The upper and lower limits of the CGC calculation by Fujii *et al* are in blue at forward rapidity.**

$R_{p\mathrm{Pb}}(y)$ for J/ψ and ψ' in Comover Approach

Difference J/ψ and ψ' suppression due to larger ψ' cross section with hadrons, no nucleon absorption, includes EPS09 LO shadowing

$$R^{\psi}_{pA}(b) = \frac{\int \mathrm{d}^2 s\, \sigma_{pA}(b)\, n(b,s)\, S^{sh}_{\psi}(b,s)\, S^{\mathrm{co}}_{\psi}(b,s)}{\int \mathrm{d}^2 s\, \sigma_{pA}(b)\, n(b,s)}$$

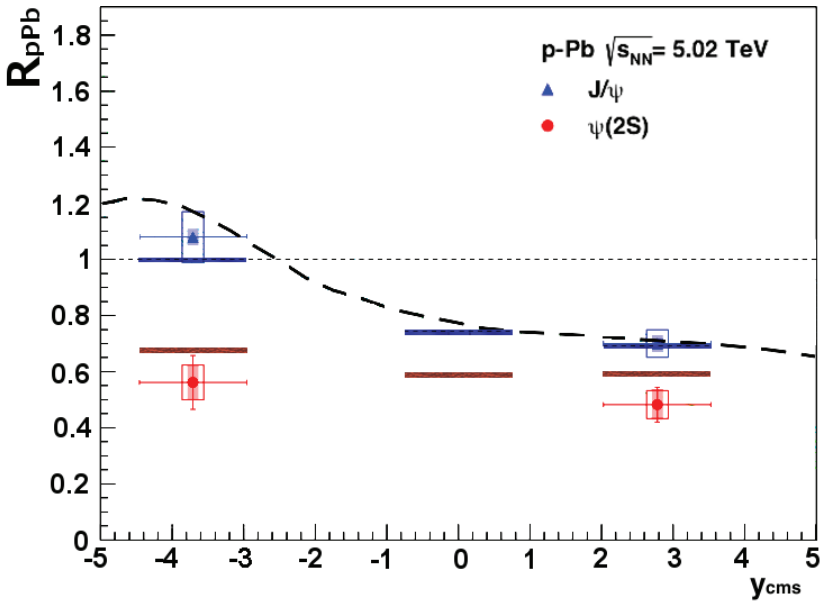

Figure 10: **The J/ψ (blue lines) and $\psi(2S)$ (red lines) nuclear modification factor R_{pPb} as a function of rapidity compared to the ALICE data (JHEP 1412 (2014) 073). The suppression due to shadowing alone (dashed line) is also shown. The ALICE results are given by the points.**

Z^0 bosons

Dependence on p_T

NLO pQCD calculations (BW Zhang *et al.*) reproduces the p_T dependence of the ATLAS and CMS data although rapidity distribution of CMS is somewhat better described

pQCD calculation including resummation (Kang and Qiu) emphasizes lower p_T region where data are well explained

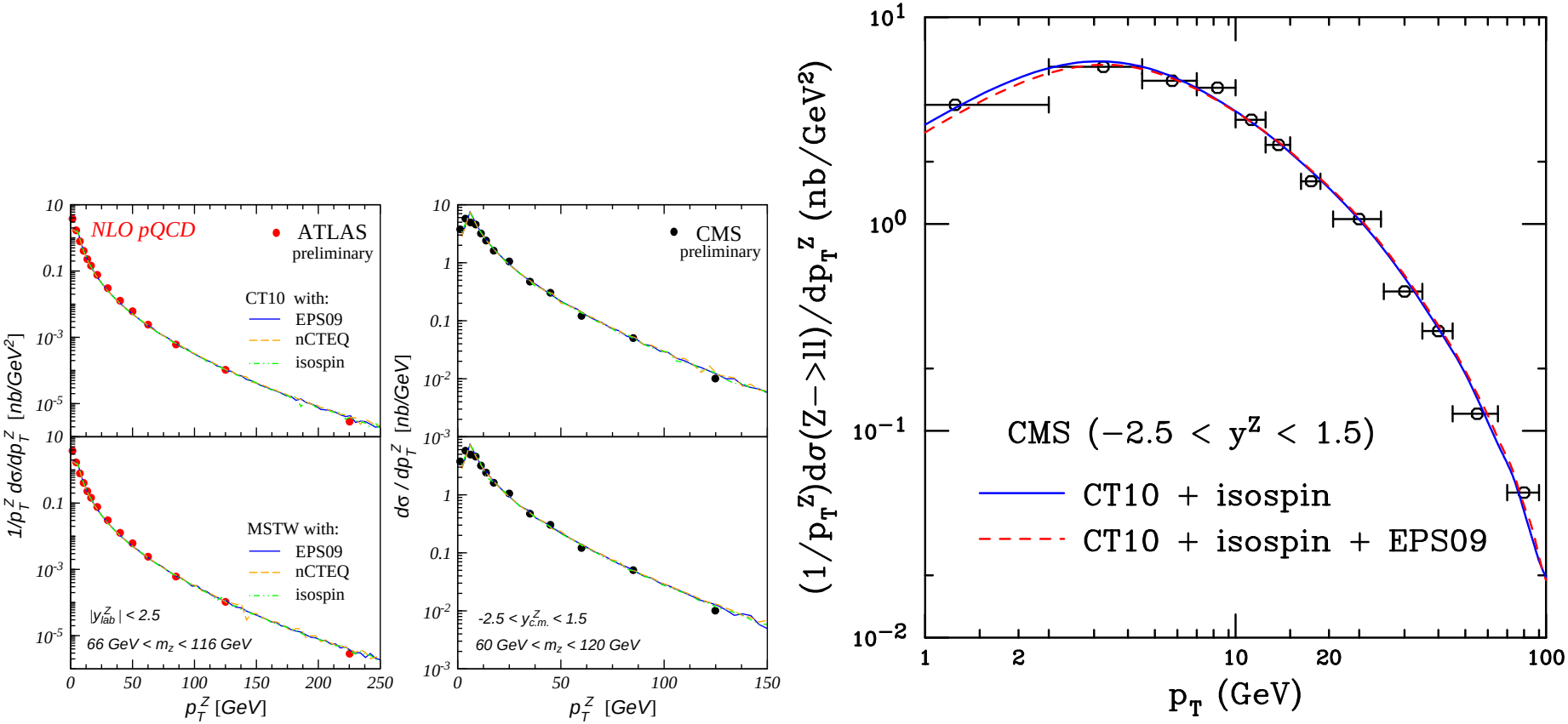

Figure 11: The differential cross section of the Z^0 rapidity in p+Pb collisions at $\sqrt{s_{NN}} = 5.02$ TeV. The left panels show the results for ATLAS (Nucl. Phys. A **931** (2014) 617) while the right show those for CMS (Nucl. Phys. A **931** (2014) 718). The top panel results are calculated with CT10 PDFs, while the bottom are calculated with MSTW2008. The left-hand side shows the p_T distributions while the rapidity distributions are on the right-hand side.

Forward-Backward Asymmetry as Discriminator?

The forward-backward asymmetry for CMS, near midrapidity, is well reproduced, with higher statistics, could discriminate

The LHCb data, at higher rapidity, are not well reproduced at backward rapidity, large difference in R_{FB}, may be due to small data set

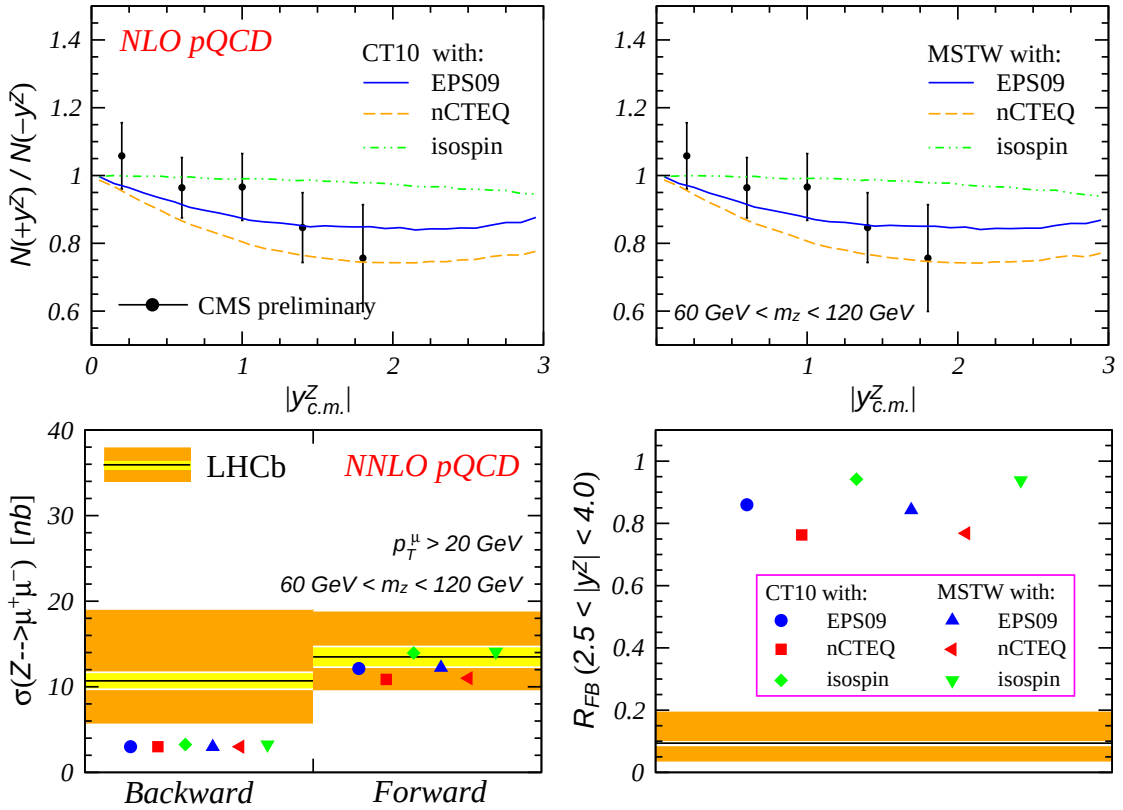

Figure 12: The forward-backward asymmetry, as a function of the absolute value of Z^0 rapidity in the center of mass frame in p+Pb collisions at $\sqrt{s_{NN}} = 5.02$ TeV. (Top) The results with the CT10 (left) and MSTW2008 PDFs (right) are shown with the CMS data (Nucl. Phys. A **931** (2014) 718). (Bottom) The forward and backward cross sections (left) and forward-backward asymmetry (right) for Z^0 production in LHCb (JHEP **1409** (2014) 030). (Calculations by B.-W. Zhang *et al.*.)

Summary

- p+Pb run at LHC provides critical studies of cold matter effects in a new energy regime
- The charged particle results for $R_{p\mathrm{Pb}}$ are mostly compatible with pQCD and CGC results, $dN_{\mathrm{ch}}/d\eta$ in CGC approach sensitive to minijet mass
- The J/ψ and Υ results are compatible with both shadowing only and energy loss only but not really with CGC+CEM
- Dijet and gauge boson results under good control although LHCb forward-backward Z^0 ratio at higher rapidity more difficult to explain with calculations but more data are needed
- This year's $p+p$ run at 5 TeV will replace interpolated baselines with measured ones, perhaps clarifying some results
- Future p+Pb run at higher energy will have lots of $p+p$ data for comparison
- Thanks again to everyone who provided predictions and data!